Computer simulation of time-gated transillumination and reflection of biological tissues and tissuelike phantoms

Michielsen, K.; Raedt, H. De; García, N.

Published in:
Medical Physics

DOI:
10.1118/1.597955

Computer simulation of time-gated transillumination and reflection of biological tissues and tissuelike phantoms

K. Michielsen and H. De Raedt[a)]
Institute for Theoretical Physics and Materials Science Centre, University of Groningen, Nijenborgh 4, NL-9747 AG Groningen, The Netherlands

N. García[b)]
Laboratorio de Física de Sistemas Pequeños y Nanotecnologia, Consejo Superior de Investigaciones Científicas, Serrano 144, Madrid E-28006, Spain

(Received 16 January 1997; accepted for publication 19 August 1997)

A simulation technique is employed to explore the possibility of locating millimeter-sized objects, immersed in turbid media, from time-gated measurements of the transmitted or reflected light. The simulation results for tissuelike phantoms are compared to experimental transillumination data and excellent agreement is found. Simulations of time-gated reflection experiments show that it is possible to detect objects of 1 mm diameter. This may open new possibilities for medical diagnosis of breast cancer in an early stage. © *1997 American Association of Physicists in Medicine.* [S0094-2405(97)00611-1]

Key words: optical transillumination, time-resolved imaging, diffusion equation, breast cancer

I. INTRODUCTION

Noninvasive diagnostic methods for detection of breast cancer at an early stage are of great importance. A successful screening method should be able to distinguish small tumors from surrounding healthy tissue before metastasis occurs.[1] The ultimate goal is to image millimeter-sized objects in 40–100 mm thick human tissue. In addition, the potential risk of contracting cancer from repeated exposure to ionizing radiation has increased the interest in noninvasive optical techniques that utilize near-infrared light. Near-infrared light can be used to look at the structure and function of biological systems.[2] In contrast to x-ray mammography where in general the incident x rays are scattered at most once, near-infrared light (with wavelengths in the 650–1300 nm range) traversing mammalian tissue is scattered strongly but is only weakly absorbed. In mammalian tissue the scattering factor is of the order of 1 mm^{-1} whereas the absorption factor is of the order of 0.01 mm^{-1}.[3,4] The main problem of imaging with diffuse light stems from the overwhelming scatter of light.

Amplitude-modulated light injected into a scattering medium generates diffusive light-intensity waves.[5] These waves have been shown to behave, in many respects, like propagating waves.[5–11] Inverse scattering techniques in combination with perturbation schemes have been employed to compute spatial variations in the absorption factor $\mu_a(\mathbf{r})$ and diffusion coefficient $D(\mathbf{r})$ (and hence the location of the objects) from the knowledge of the phase and amplitude of these waves at various source and detector positions.[12] Recently the reconstruction from experimental data of two 10 mm diameter perfectly absorbing spheres immersed in Intralipid has been demonstrated.[12]

Picosecond time-scale imaging techniques have been used to detect objects immersed in highly scattering media.[13–16] A systematic study of the time-gating technique has shown that it is highly sensitive with respect to spatial variations in the absorption or scattering factors,[14] in particular under conditions that are similar to those of biological systems of interest.[14] Recent experiments show that the spatial resolution of the time-gating technique can also be obtained with the absorption method.[17]

The diffusive character of the light transport through turbid media usually prohibits the direct detection of weakly absorbing objects hidden in the medium by direct continuous-wave measurement of the transmitted or reflected light intensity. Only if the diffusion factors of the object and the medium differ considerably is direct detection possible.[18] In the diffusive regime, the strong scattering by the medium blurs the variations in the transmitted or reflected light resulting from the local (small) variations of the absorption and the diffusion factor caused by an object immersed in the medium.

II. MODEL

Most of the light entering a turbid medium (possibly containing one or more small objects with reduced scattering and/or absorption factors different from that of the medium) is scattered many times before it reaches the detector. For weakly absorbing media the propagation of these photons is, to a good approximation, described by the time-dependent diffusion equation[19–21] (TDDE)

$$\frac{\partial I(\mathbf{r},t)}{\partial t} = \nabla \cdot D(\mathbf{r}) \nabla I(\mathbf{r},t) - v\,\mu_a(\mathbf{r}) I(\mathbf{r},t) + S(\mathbf{r},t), \qquad (1)$$

where $I(\mathbf{r},t)$ is the light intensity at a point $\mathbf{r}$ and at time t, $D(\mathbf{r}) = v/3(\mu_s'(\mathbf{r}) + \mu_a(\mathbf{r}))$ is the diffusion coefficient, $\mu_s'(\mathbf{r})$ is the reduced scattering factor, $\mu_a(\mathbf{r})$ denotes the absorption factor and v is the velocity of light in the medium in the absence of objects. The light source is represented by $S(\mathbf{r},t)$. The presence of objects in the medium is reflected by spatial

variations in the absorption factor and/or reduced scattering factor (and hence also in the diffusion coefficient). In general, both the absorption and reduced scattering factor will fluctuate randomly around their spatial average, denoted $\overline{\mu_a}$ and $\overline{\mu_s'}$, respectively. For weakly absorbing media $\overline{\mu_a} \ll \overline{\mu_s'}$.

We have developed software to simulate the time-gating experiments, based on a numerical method to solve the TDDE (1). In this paper we demonstrate that the simulation technique yields results that are in excellent agreement with experiment.[14] We then use the technique to determine the conditions under which a small, weakly absorbing object might be detected by measuring the transmitted and/or reflected light intensity.

III. ALGORITHM

According to Eq. (1) the time evolution of the light intensity at time $t+\tau$ is related to the light intensity at time t through

$$I(\mathbf{r},t+\tau)=e^{-\tau H}\left[I(\mathbf{r},t)+\int_0^\tau d\tau'\ e^{\tau' H}S(\mathbf{r},t+\tau')\right], \qquad (2)$$

where τ denotes the time step, $H=-\nabla\cdot D(r)\nabla+V(\mathbf{r})$, and $V(\mathbf{r})=v\mu_a(\mathbf{r})$. From Eq. (2) it follows that all we need to solve the TDDE (1) is an algorithm to compute $e^{-\tau H}A(\mathbf{r})$ for arbitrary $A(\mathbf{r})$.

We have developed an algorithm to compute $e^{-\tau H}A(\mathbf{r})$, based on the fractal decomposition of matrix exponentials proposed by Suzuki.[22] The algorithm is accurate to second order in the spatial mesh size δ and to fourth order in the temporal mesh size τ. Conceptually the algorithm is closely related to the one we have developed for the time-dependent Schrödinger equation.[23] The first step in setting up a numerical method to solve the TDDE (1) is to discretize the derivatives with respect to the spatial coordinates. The simplest approximation scheme having satisfactory properties is[24]

$$\begin{aligned}K_x I(\mathbf{r},t)\equiv&-\frac{\partial}{\partial x}\left(D(\mathbf{r})\ \frac{\partial}{\partial x}\ I(r,t)\right)\Big|_{\mathbf{r}=(i\delta,j\delta,k\delta)}\\ \approx&-\frac{D_{i+1,j,k}+D_{i,j,k}}{2\delta^2}\ I_{i+1,j,k}\\ &+\frac{D_{i+1,j,k}+2D_{i,j,k}+D_{i-1,j,k}}{2\delta^2}\ I_{i,j,k}\\ &-\frac{D_{i-1,j,k}+D_{i,j,k}}{2\delta^2}\ I_{i-1,j,k},\end{aligned} \qquad (3)$$

where $I_{i,j,k}=I(\mathbf{r}=(i\delta,j\delta,k\delta))$ and $D_{i,j,k}=D(\mathbf{r}=(i\delta,j\delta,k\delta))$. For the derivatives with respect to y and z we use expressions similar to Eq. (3).

In analogy with the time-dependent Schrödinger equation, the time-step operator $e^{-\tau H}$ is approximated by a product of matrix exponentials. An approximation correct to second order in the time step τ is given by[25,26]

$$e^{-\tau H}\approx e^{-\tau K_z/2}e^{-\tau K_y/2}e^{-\tau K_x/2}e^{-\tau V}e^{-\tau K_x/2}e^{-\tau K_y/2}e^{-\tau K_z/2}. \qquad (4)$$

Instead of using fast Fourier transform techniques[27] to compute the quantities such as $e^{-\tau K_x/2}A(\mathbf{r})$, we replace $e^{-\tau K_x/2}$ by a first-order product formula approximation and obtain[28]

$$\begin{aligned}e^{-\tau K_x/2}\approx&X(\tau/2)\\ =&\prod_{j,k}\left[\prod_{i\in\mathscr{E}}\ \frac{1}{2}\begin{pmatrix}1+e^{-\tau a_{i,j,k}} & 1-e^{-\tau a_{i,j,k}}\\ 1-e^{-\tau a_{i,j,k}} & 1+e^{-\tau a_{i,j,k}}\end{pmatrix}^{(i,i+1)}\right]\\ &\times\left[\prod_{i\in\mathscr{O}}\ \frac{1}{2}\begin{pmatrix}1+e^{-\tau a_{i,j,k}} & 1-e^{-\tau a_{i,j,k}}\\ 1-e^{-\tau a_{i,j,k}} & 1+e^{-\tau a_{i,j,k}}\end{pmatrix}^{(i,i+1)}\right],\end{aligned} \qquad (5)$$

where the triples (i,j,k) appearing in Eq. (5) represent a point on the lattice, $\mathscr{E}$ and $\mathscr{O}$ are the sets of even and odd numbers, respectively, and $a_{i,j,k}=\delta^{-2}(D_{i,j,k}+D_{i+1,j,k})/2$. The superscripts $(i,i+1)$ labeling the two-by-two matrices indicate that this matrix operates on the vector $(I_{i,j,k},I_{i+1,j,k})$ only. In Eq. (4) we replace $e^{-\tau K_y/2}$ and $e^{-\tau K_z/2}$ by similar approximations, $Y(\tau/2)$ and $Z(\tau/2)$, respectively. The resulting product formula remains correct to order τ^2. It is also of interest to note that all the matrix elements of both $e^{-\tau K_x/2}$ and $X(\tau/2)$ are positive so that approximation (5) has the desirable feature that it will never lead to negative light intensities.

For $V(\mathbf{r})\geqslant 0$ (the case of interest) the explicit, second-order algorithm defined by

$$\begin{aligned}e^{-\tau H}\approx&S_2(\tau)\\ =&Z(\tau/2)Y(\tau/2)X(\tau/2)e^{-\tau V}X(\tau/2)Y(\tau/2)Z(\tau/2)\end{aligned} \qquad (6)$$

is unconditionally stable. Indeed, if $\|M\|$ denotes the eigenvalue of the matrix M of largest absolute value, we have

$$\|Z(\tau/2)Y(\tau/2)X(\tau/2)e^{-\tau V}X(\tau/2)Y(\tau/2)Z(\tau/2)\|\leqslant 1, \qquad (7)$$

which is the condition expressing numerical stability of the scheme.[24]

The accuracy of the second-order algorithm may be insufficient if we want to solve the TDDE for long times. In practice this is only a minor complication because the second-order algorithm can be reused to build an algorithm that is correct to fourth order in the time step. According to Suzuki's fractal decomposition,[22]

$$S_4(\tau)=S_2(p\tau)S_2(p\tau)S_2((1-4p)\tau)S_2(p\tau)S_2(p\tau) \qquad (8)$$

will be an approximation to the time-step operator that is correct to fourth order in τ provided $p=(4-4^{1/3})^{-1}$. In our simulations we have used Eqs. (6) and (8) and obtained quantitatively similar results.

The contribution from the source $S(\mathbf{r},t)$ is computed using the standard Simpson rule[29]

$$\begin{aligned}&e^{-\tau H}\int_0^\tau d\tau'\ e^{\tau' H}S(\mathbf{r},t+\tau')\\ &\quad\approx\frac{\tau}{6}\left(e^{-\tau H}S(\mathbf{r},t)+4e^{-\tau H/2}S\left(\mathbf{r},t+\frac{\tau}{2}\right)+S(\mathbf{r},t+\tau)\right),\end{aligned} \qquad (9)$$

which is correct to fourth order in τ.

From the structure of Eq. (4) and $S_2(\tau)$ it is clear that the propagation of light over a time-step τ has been reduced to elementary operations: repeated multiplications of two elements of a vector by the corresponding two elements of another vector (in the case of $e^{-\tau V}$), or of matrix-vector multiplications involving two-by-two matrices only. The resulting algorithm is fast, stable and flexible. For practical applications to the tumor detection problem it is important that the software can deal with irregularly shaped samples. As the Suzuki-product-formula-based algorithm presented above operates on numbers labeled by real-space indices only, it is as easy to solve the TDDE for a particular shape as it is to solve the TDDE for a rectangular box.

IV. SIMULATION SOFTWARE

Our current version of the software solves Eq. (1) in two and three dimensions subject to perfectly reflecting and/or absorbing boundary conditions. To mimic realistic situations, the algorithm can deal with spatial variations of the reduced scattering and/or absorption coefficients of the medium (e.g., tissue) and/or objects (e.g., tumors) as well as random fluctuations of all these quantities. The light intensity transmitted by the sample is being collected by detectors located at $\mathbf{r}=(L_x,y,z)$, where L_x denotes the size of the rectangular simulation box in the direction of the incident light. The reflected light intensity is being recorded at $\mathbf{r}=(0,y,z)$. The light source is placed at $x=0$ [i.e., $S(\mathbf{r},t)=0$ unless $\mathbf{r}=(0,y,z)$]. We have carried out simulations using sources of variable size, including the cases of a point source $[S(\mathbf{r},t)=S_0(t)\delta(x)\delta(y-y_0)\delta(z-z_0)]$ and uniform illumination $[S(\mathbf{r},t)=S_0(t)\delta(x)]$. At $t=0$ the source starts to illuminate the system, until $t=t_p$, when it is turned off. Detection of the light intensity starts at $t_d(t_d>t_p)$. Our simulation software allows the detectors to record the instantaneous or the time-integrated light intensity.

For a representative sample of 70 mm×70 mm, using a mesh size of $\delta=1$ mm($L_x=L_y=71$), it takes about 1 min on a Pentium Pro 200 MHz system to carry out 1000 time steps, including data analysis and visualization. The CPU time required to solve the TDDE by the algorithm presented above scales linearly with the number of time steps and the total number of grid points. Calculation of the time evolution of the light intensity for a grid of $63\times63\times63=250\,047$ points and 1480 time steps takes 6 min on a Cray C98 (single processor), 42 min on a SGI Power Challenger (single processor), and 65 min on an IBM RS/6000 model 43P workstation. For exploratory purposes it is advantageous to simulate two-dimensional (2D) systems. Then, for selected cases, we simulate the corresponding three-dimensional (3D) system. On a qualitative level there seems to be little difference between the results obtained from 2D or 3D simulations.

As the effect of particular implementations, compilers, and computer systems on the performance of specific simulation algorithms can be substantial, it is difficult to compare different approaches on a quantitative basis but it may be of interest to compare, on a conceptual level, our approach with others. Techniques that have been developed to calculate light propagation in turbid media can be classified into stochastic methods, such as the Monte Carlo (MC) simulations[30–35] and random walk models,[36,37] or deterministic methods that are based on the solutions of the diffusion equation, which in highly scattering media approximates to the transport equation.[19]

The MC simulations trace a large number of individual paths of photons propagating through a scattering medium. The scattering events are determined by a probability function that matches the scattering coefficient. At each scattering event part of the photons are absorbed. The amount of absorption is determined by the absorption coefficient. The scattering angle is given by the scattering phase function. A MC algorithm has the advantages of being conceptually simple and of being flexible with respect to geometry, phase functions, and boundary conditions. A disadvantage of MC simulations is the large amount of computer time needed to obtain statistically good quality data.

In general, the numerical methods based on the solution of the diffusion equation are much faster than the MC methods to describe the light propagation in tissue, if the scattering and absorption mechanisms allow the use of the diffusion approximation.

The diffusion equation, including its time-dependent form, can be solved analytically for a homogeneous medium and rather simple geometries.[5,38] More flexible than the analytical methods are the numerical methods, such as the finite element method (FEM),[39–41] the finite difference method (FDM)[42] and our method proposed above. The basic idea of the FEM is that a model that satisfies the time-independent diffusion equation is divided into elements, and an approximate solution to the equation is calculated over each element. The solution for the whole model can be derived from the algebraic solutions for each element. The mean time of flight can be calculated directly from the first moment of the time-dependent light intensity.[41] Using the FDM, the diffusion equation is converted into a finite difference equation for finite steps of the spatial variables and the temporal variable. The algorithm we use is identical to the FDM as far as the treatment of the spatial variables is concerned.

V. COMPARISON WITH EXPERIMENTS

In order to compare with the experimental results of Mitic *et al.*[14] we have made simulations for systems of size 40 mm×127 mm, with the model parameters taken from Ref. 14. Unless mentioned explicitly, the mesh size of the spatial discretization $\delta=1$ mm, the time step $\tau=1$ ps, $t_p=7$ ps, $t_d=350$ ps, and the speed of light in the medium $v=0.222$ mm/ps. We have checked (by reducing the mesh size and the time step) that the numerical results are, for all practical purposes, exact. The simulation itself is carried out in a manner identical to the procedure used in the time-gating technique.[14] The sample is illuminated uniformly by the pulsed light-source. This corresponds to the experimental situation in which the phantom is located on an $x-y$ stage and is moved in the horizontal plane under computer

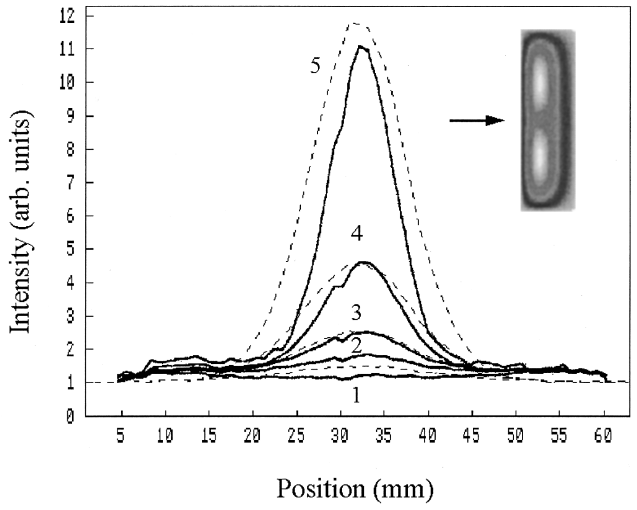

FIG. 1. Comparison of experimental (Ref. 14) (solid lines) and computer simulation (dashed lines) results for the time-gated transilluminated diffusive light intensity. In experiment and simulation the turbid medium has a reduced scattering factor $\mu_s' = 0.9\ \mathrm{mm}^{-1}$ and an absorption factor $\mu_a < 0.001\ \mathrm{mm}^{-1}$; the absorption factor of the 8 mm diameter tube $\mu_a = 0.014\ \mathrm{mm}^{-1}$ (Ref. 14). The reduced scattering factor inside the object $\mu_s' = 0$. As in Ref. 14 [Fig. 12(a)], 1: continuous wave case (experimental data only); 2: $\Delta t = 960$ ps; 3: $\Delta t = 480$ ps; 4: $\Delta t = 240$ ps; 5: $\Delta t = 30$ ps. The inset shows the light distribution inside the sample for $\Delta t = 960$ ps, the arrow indicates the direction of the incident light. See also Fig. 12(a) of Ref. 14.

control.[14] The detector accumulates the light intensity over the interval $t_d < t < t + \Delta t$ where Δt denotes the time gate.

In Fig. 1 we depict our simulation results (dashed lines) and the experimental data (solid lines) that are taken from Ref. 14 (Fig. 12a of Ref. 14). The medium contains a plastic tube (8 mm diameter) filled with diluted ink, positioned in the center of the sample. In the simulation both the absorption and the scattering factor are allowed to fluctuate randomly within 10% of their values quoted in Ref. 14. Our numerical results are in remarkably good agreement with the experimental data. The inset shows the distribution of light inside the sample at $\Delta t = 960$ ps. The object is clearly visible.

Increasing the absorption factor of the diluted ink by a factor of 9 (Fig. 12b of Ref. 14) yields the results shown in Fig. 2. Again the overall agreement with the experimental[14] data is excellent. Simulation and experimental[14] data for a medium containing bead pairs are shown in Fig. 3. The agreement between experiment and theory is remarkable, taking into account that no attempt has been made to make a ''best'' fit. Figure 4 displays the results for a system containing a plastic tube with ink-tinted milk with the same scattering factor as the medium but with a different absorption factor. Clearly the simulation data displays all the features observed in experiment, in particular the full-width at half-maximum agrees very well with the experimental value. The above simulation results and others (not shown) demonstrate that our simulation software reproduces all the features observed in the experiments on the tissuelike phantoms reported in Ref. 14.

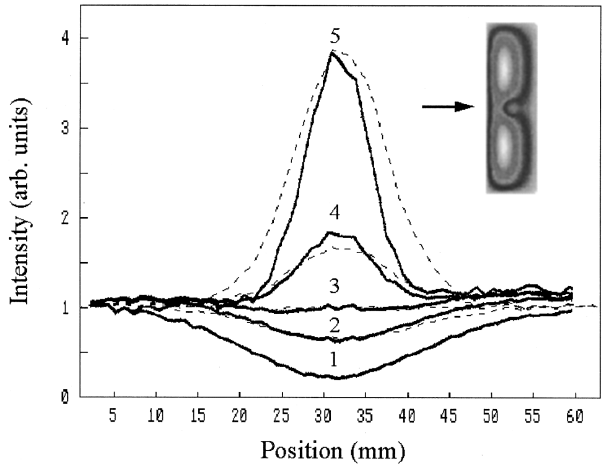

FIG. 2. Same as Fig. 1 except that the absorption factor of the 8 mm diameter tube $\mu_a = 0.13\ \mathrm{mm}^{-1}$ (Ref. 14). See also Fig. 12(b) of Ref. 14.

VI. SIMULATION OF TIME-GATED REFLECTION EXPERIMENTS

Our simulation software reproduces, without fitting, the data obtained from time-gated transillumination measurements on turbid media containing relatively large (± 8 mm diameter) objects. Hence it can be used to explore different techniques for improving the detection methods. We have used our simulation method to devise a data processing technique to enhance the imaging quality. An obvious approach is to compare the data with other data obtained from a reference, or model system. In the case at hand we know that the immense scattering of light is responsible for the blurring of the images of the objects. The variations of both the reduced scattering and absorption factor due to the objects are relatively small. Therefore as a starting point, it is reasonable to take as a reference model a system with a constant diffusion coefficient. In practice the data processing method works as follows: We measure the integrated intensity I of

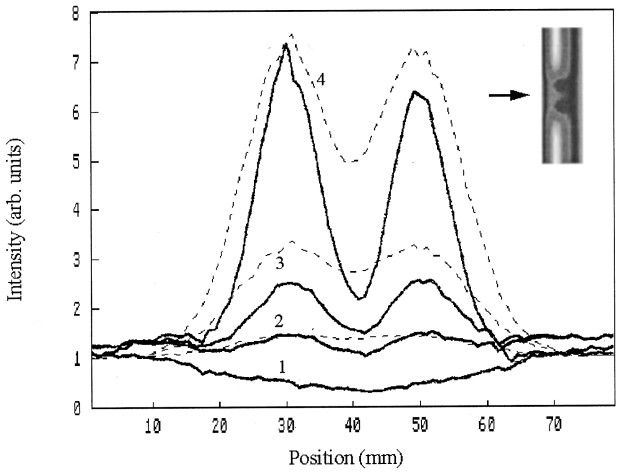

FIG. 3. Same as Fig. 1 except that instead of one there are two 10 mm diameter objects, separated by 20 mm, with an absorption factor $\mu_a = 0.029\ \mathrm{mm}^{-1}$ (Ref. 14). See also Fig. 13(a) of Ref. 14.

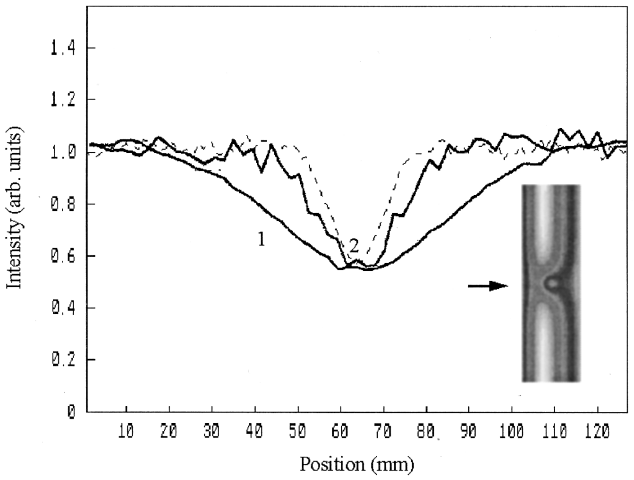

FIG. 4. Same as Fig. 1 except that the turbid medium has a reduced scattering factor $\mu_s'=0.8\ \mathrm{mm}^{-1}$ and that the absorption and reduced scattering factor of the 8 mm diameter tube are $\mu_a=0.1\ \mathrm{mm}^{-1}$ and $\mu_s'=0.8\ \mathrm{mm}^{-1}$, respectively (Ref. 14). See also Fig. 15 of Ref. 14.

the sample, divide this intensity by the reference signal I_0 as obtained from a simulation of a reference model, and compute $\ln(I/I_0)$ for various source and detector positions. According to a generalization[43] of inequalities due to Symanzik,[44] the resulting distribution should reveal whether there are hidden objects or not.

An illustration of the usefulness of this image processing method is given in Figs. 5–9. Unless explicitly mentioned otherwise, the spatial mesh size $\delta=1$ mm, the time step $r=1$ ps, the source pulse time $t_p=10$ ps, the time at which the detectors start to record intensity $t_d=500$ ps, and the speed of light in the medium $v=0.222$ mm/ps. Guided by the experiments on breast tissue,[3,14,45–47] in our simulations we will assume that the turbid medium is characterized by an absorption and reduced scattering factor $\mu_a=0.01\ \mathrm{mm}^{-1}$ and $\mu_s'=0.9\ \mathrm{mm}^{-1}$, respectively. For tumor tissue we will take $\mu_a=0.1\ \mathrm{mm}^{-1}$ and $\mu_s'=0.9\ \mathrm{mm}^{-1}$, unless explicitly mentioned otherwise.

We will use the shorthand notation $\overline{I_T}$ and $\overline{I_R}$ for the transmitted and reflected intensity, respectively, integrated over the corresponding detection area. All intensities given below are normalized with respect to the light intensity supplied by the source.

In Fig. 5 we show results of a simulation for a sample of size 71 mm×71 mm, containing an object of 2.5 mm radius, positioned at (36,26) mm. The sample is illuminated by a source of diameter 1 mm centered around (0,36) mm. In the sequel we will call such a small source a point source. Figures 5(a) and 5(c) show the integrated intensity while Figs. 5(b) and 5(d) show the corresponding processed signal. For $\Delta t=612$ ps [Figs. 5(a) and 5(b)], it is clear that the object leaves no trace in the transmitted and reflected intensity whereas the processed data clearly indicate that there is an object inside the sample. For $\Delta t=1836$ ps [Figs. 5(c) and 5(d)] the transmitted intensity shows an asymmetry. Since the light source is positioned at (0,36) mm, this asymmetry indicates that there is an object immersed in the sample. In the reflected intensity, however, the object leaves no trace. In the processed reflected intensity the object is clearly visible. Note that the position of the maximum of the processed intensity changes with Δt [Figs. 5(b) and 5(d)].

Figures 6(a) and 6(b) show simulation results for the same setup as the one used for Figs. 5(c) and 5(d) except that the light source is now positioned at (0,16) mm. The transmitted and reflected intensities in Figs. 5(c) and 5(d) and Figs. 6(a) and 6(b) look completely different. As the image of the point source itself resembles the image of an object it is as good as

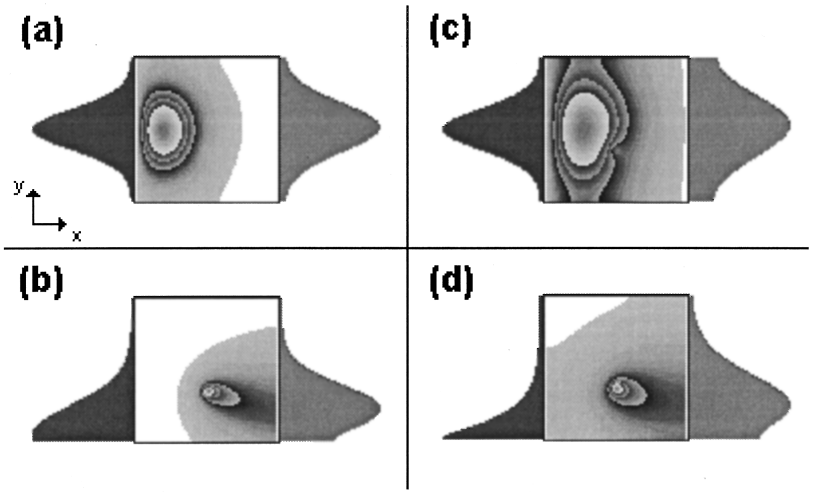

FIG. 5. Simulation of a time-resolved experiment on a turbid medium with a reduced scattering factor $\mu_s'=0.9\ \mathrm{mm}^{-1}$ and an absorption factor $\mu_a=0.01\ \mathrm{mm}^{-1}$ containing a 2.5 mm radius object with absorption and reduced scattering factors $\mu_a=0.1\ \mathrm{mm}^{-1}$ and $\mu_s'=0.9\ \mathrm{mm}^{-1}$, respectively. The dimensions of the sample are 71 mm×71 mm. The object is located at (36,26) mm. The sample is illuminated by a source of diameter 1 mm centered around (0,36) mm during a time $t_p=10$ ps. (a) Time-integrated transmitted (right) and reflected (left) intensity for $\Delta t=612$ ps. $\overline{I_T}\approx 0.6\times10^{-8}$ and $\overline{I_R}\approx 0.2\times10^{-2}$; (b) processed signal corresponding to (a); (c) same as (a) except that $\Delta t=1836$ ps. $\overline{I_T}\approx 0.5\times10^{-6}$ and $\overline{I_R}\approx 0.3\times10^{-2}$; (d) processed signal corresponding to (c). The (processed) light intensities inside the sample are also shown.

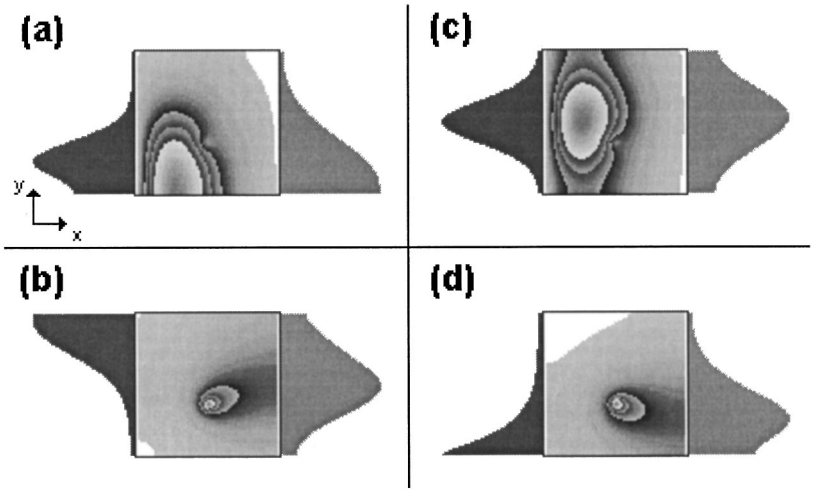

FIG. 6. Same as Fig. 5 except for the source illuminating the system. $\Delta t = 1836$ ps. (a) Point source centered around (0, 16) mm. $\overline{I_T} \approx 0.5 \times 10^{-6}$ and $\overline{I_R} \approx 0.3 \times 10^{-2}$; (b) processed signal corresponding to (a); (c) source emitting a Gaussian light distribution of width 5 mm, centered around (0, 36) mm. $I_T \approx 0.5 \times 10^{-6}$ and $I_R \approx 0.3 \times 10^{-2}$; (d) processed signal corresponding to (c).

impossible to conclude from the transmitted or reflected intensities whether or not there is an object inside the sample. The processed intensities, however, correctly signal the presence of an object. From Figs. 5, 6(a) and 6(b), it follows that there is no obvious relationship between the position of the object and the maximum of the processed intensity.

Illumination of the sample by a source emitting a Gaussian light distribution of width 5 mm yields the results shown in Figs. 6(c) and 6(d). These results can hardly be distinguished from those shown in Figs. 5(c) and 5(d) obtained by using a point source. Figure 7 displays results for a system containing an object of 2.5 mm radius, positioned at (16,26) mm. Figs. 7(a) and 7(b) show the time-integrated transmitted and reflected intensities for illumination by a point source while Figs. 7(c) and 7(d) show the intensities for uniform illumination of the whole left edge of the sample. Using a point source yields no trace of the object in the reflected intensity and only a weak one in the transmitted intensity [Figs. 5(a) and 5(c) and 7(a)]. In the processed signals, however, there is a clear signal of the object [Figs. 5(b) and 5(d) and 7(b)]. Uniform illumination of the whole left edge of the sample [Figs. 7(c) and 7(d)] yields a very weak signal of the object in the transmitted and reflected intensities and a clear signal in the processed intensities. The fingerprint of the object in the reflected intensity disappears completely if the object is more than 20 mm away from the entrance plane, while in the transmitted intensity the very weak signal is present, independent of the location of the object within the sample (results not shown). In the case of uniform illumination the position of the maximum of the processed intensity no longer changes as a function of time (not shown) and corresponds to the y coordinate of the position of the object.

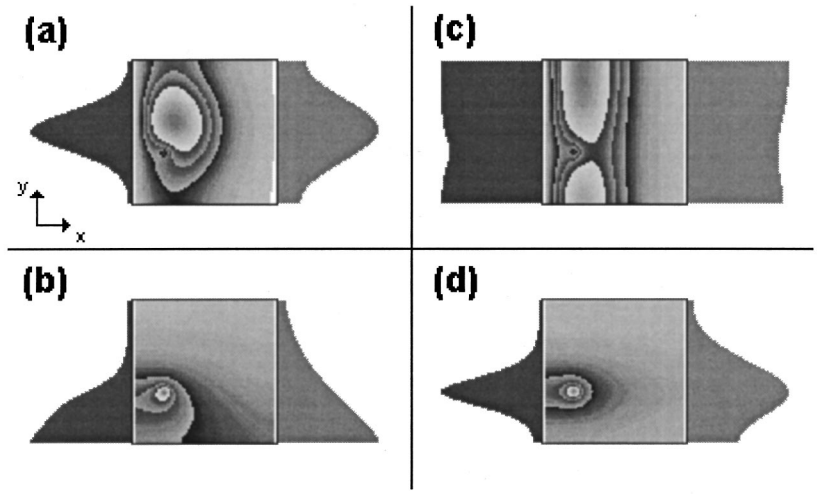

FIG. 7. Same as Fig. 5 except for the source illuminating the system and the position of the object (16,26) mm $\Delta t = 1836$ ps. (a) Point source centered around (0,36) mm. $\overline{I_T} \approx 0.6 \times 10^{-6}$ and $\overline{I_R} \approx 0.2 \times 10^{-2}$; (b) processed signal corresponding to (a); (c) uniform illumination of the left edge of the sample. $\overline{I_T} \approx 0.6 \times 10^{-6}$ and $I_R \approx 0.2 \times 10^{-2}$; (d) processed signal corresponding to (c).

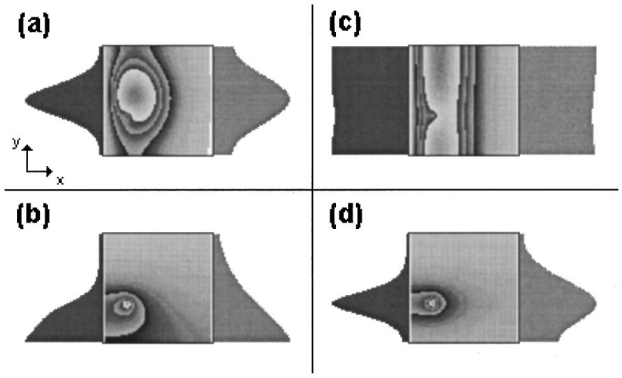

FIG. 8. Same as Fig. 7 except that the object has a radius of 0.5 mm.

Uniform illumination of the other edges of the sample should therefore allow the determination of the position of the object.

In Fig. 8 we present simulation results for a system containing an object of 0.5 mm radius. For comparison the setup is kept the same as the one used for Fig. 7. As seen from Fig. 8(a), using a point source, it is no longer possible to detect the object in the transmitted intensity. Also for uniform illumination of the whole left edge of the sample the fingerprint of the small object in the transmitted and reflected intensities [Fig. 8(c)] is much weaker than for an object of radius 2.5 mm [Fig. 7(c)]. In the simulation the object always leaves a trace in the processed signals, independent of its location in the sample. Evidently, due to the signal-to-noise ratio, this will not necessarily be the case in experiment. From Figs. 7 and 8 it is clear that it is very difficult, not to say impossible, to infer the size of the object from the measured intensities.

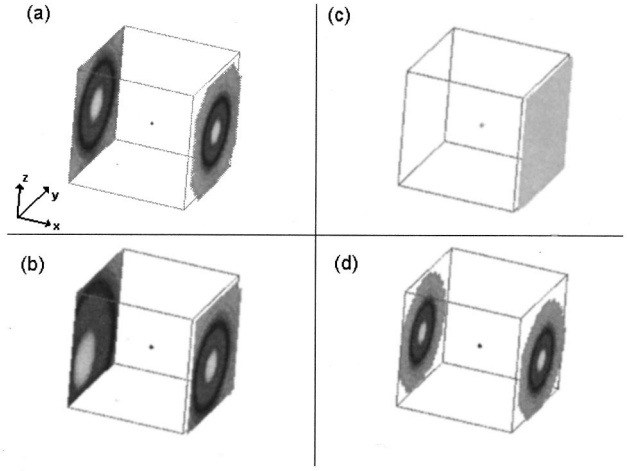

FIG. 9. Simulation of a time-gated transillumination and reflection experiment on a turbid medium with a reduced scattering factor $\mu_s' = 1\ \mathrm{mm}^{-1}$ and an absorption factor $\mu_a' = 0.01\ \mathrm{mm}^{-1}$ containing a 1 mm radius sphere with an absorption and a reduced scattering factor of $\mu_a = 0.1\ \mathrm{mm}^{-1}$ and $\mu_s' = 1\ \mathrm{mm}^{-1}$, respectively. The dimensions of the sample are $63\ \mathrm{mm} \times 63\ \mathrm{mm} \times 63\ \mathrm{mm}$, $\Delta t = 796$ ps, and $t_d = 500$ ps. The object is located at $(x,y,z) = (32\ \mathrm{mm}, 30\ \mathrm{mm}, 34\ \mathrm{mm})$. The small sphere inside the sample denotes the position of the object. (a) Time-integrated intensity transmitted (right) and reflected (left) intensity. The sample is illuminated by a source of diameter 1 mm centered around (0, 32, 32) mm during a time $t_p = 10$ ps; (b) processed signal corresponding to (a); (c) same as (a) except that the sample is uniformly illuminated on its whole left plane; (d) processed signal corresponding to (c). The light gray, black, and dark gray areas receive respectively more than 70%, between 40% and 70%, and less than 40% of the detected light.

In Fig. 9 we show a result of a simulation for a sample of size $63\ \mathrm{mm} \times 63\ \mathrm{mm} \times 63\ \mathrm{mm}$, containing a sphere of 1 mm radius, positioned at $(x,y,z) = (32\ \mathrm{mm}, 30\ \mathrm{mm}, 34\ \mathrm{mm})$. In the turbid medium $\mu_s' = 1\ \mathrm{mm}^{-1}$ and $\mu_a = 0.01\ \mathrm{mm}^{-1}$. The object has $\mu_s' = 1\ \mathrm{mm}^{-1}$ and $\mu_a = 0.1\ \mathrm{mm}^{-1}$. The light intensity transmitted by the sample is being collected by detectors located at $(63\ \mathrm{mm}, y, z)$, while the reflected light intensity is recorded at $(0,y,z)$. Figures 9(a) and 9(b) show results for illumination of the sample by a point source centered around (0,32,32) mm and Figs. 9(c) and 9(d) show the results for uniform illumination of the sample on its whole left plane. Figures 9(a) and 9(c) show the integrated intensities, while Figs. 9(b) and 9(d) show the processed signals. It is clear that the object leaves no trace in the intensity whereas the processed data clearly indicate that there is an object inside the sample. The position of the maximum of the processed reflected intensity changes with Δt if a point source is used, just as in the 2D case.

VII. CONCLUSION

We have developed software to simulate time-gated transillumination and reflection experiments of light diffusion in turbid media. Our simulation technique reproduces experimental data without the need of fitting parameters. Simulation results for the time-gated transillumination and reflection technique suggest that under conditions similar to those of human tissue with tumors, objects of 1 mm diameter can be located, independent of their location within the sample, if a data processing technique is used. The possibility of detecting objects, e.g., tumors, of 1 mm radius (or smaller) by reflection measurements offers new possibilities for performing *in vivo* experiments on breasts and brains, with the advantage of having a higher magnitude of the signal than in transillumination experiments and hence the possible advantage that there is no need to compress or deform the tissue.

ACKNOWLEDGMENTS

We are indebted to M. Nieto Vesperinas for drawing our attention to the tumor detection problem. This work is supported by EEC and Spanish research contracts.

[a]Electronic-mail: h.a.de.raedt@phys.rug.nl
[b]Electronic-mail: nikolas.garcia@fsp.csic.es

[1] J. C. Hebden, D. J. Hall, M. Firbank, and D. T. Delpy, ''Time-resolved optical imaging of a solid tissue-equivalent phantom,'' Appl. Opt. **34**, 8038–8047 (1995).
[2] J. Alper, ''Transillumination: Looking Right Through You,'' Science **261**, 560 (1993).
[3] R. Marchesini, A. Bertoni, S. Andreola, E. Melloni, and A. E. Sichirollo, ''Extinction and absorption coefficients and scattering phase functions of human tissues *in vitro*,'' Appl. Opt. **28**, 2318–2324 (1989).
[4] A. Kienle, L. Lilge, M. S. Patterson, R. Hibst, R. Steiner, and B. C. Wilson, ''Spatially resolved absolute diffuse reflectance measurements for noninvasive determination of the optical scattering and absorption coefficients of biological tissue,'' Appl. Opt. **35**, 2304–2314 (1996).

[5]J. B. Fishkin and E. Gratton, ''Propagation of photon-density waves in strongly scattering media containing an absorbing semi-infinite plane bounded by a straight edge,'' J. Opt. Soc. Am. A **10**, 127–140 (1993).
[6]M. A. O'Leary, D. A. Boas, B. Chance, and A. G. Yodh, ''Refraction of Diffuse Photon Density Waves,'' Phys. Rev. Lett. **69**, 2658–2661 (1992).
[7]D. A. Boas, M. A. O'Leary, B. Chance, and A. G. Yodh, ''Scattering and wavelength transduction of diffuse photon density waves,'' Phys. Rev. E **47**, R2999–R3002 (1993).
[8]B. J. Tromberg, L. O. Svaasand, T. T. Tsay, and R. C. Haskell, ''Properties of photon density waves in multiple-scattering media,'' Appl. Opt. **32**, 607–616 (1993).
[9]D. A. Boas, M. A. O'Leary, B. Chance, and A. G. Yodh, ''Scattering of diffuse photon density waves by spherical inhomogeneities within turbid media: Analytic solution and applications,'' Proc. Natl. Acad. Sc. USA **91**, 4887–4891 (1994).
[10]J. M. Schmitt, A. Knüttel, and J. R. Knutson, ''Interference of diffusive light waves,'' J. Opt. Soc. Am. A **9**, 1832–1843 (1992).
[11]B. Chance, K. Kang, L. He, J. Wang, and E. M. Sevick, ''Highly sensitive object location in tissue models with linear in-phase and anti-phase multi-element optical arrays in one and two dimensions,'' Proc. Natl. Acad. Sc. USA **90**, 3423–3427 (1993).
[12]M. A. O'Leary, D. A. Boas, B. Chance, and A. G. Yodh, ''Experimental images of heterogeneous turbid media by frequency-domain diffusing-photon tomography,'' Opt. Lett. **20**, 426–428 (1995).
[13]D. A. Benaron, and D. K. Stevenson, ''Optical Time-of-Flight and Absorbance Imaging of Biologic Media,'' Science **259**, 1463–1466 (1993).
[14]G. Mitic, J. Kölzer, J. Otto, E. Plies, G. Sölkner, and W. Zinth, ''Time-gated transillumination of biological tissues and tissuelike phantoms,'' Appl. Opt. **33**, 6699–6710 (1994).
[15]R. R. Alfano, X. Liang, L. Wang, and P. P. Ho, ''Time-Resolved Imaging of Translucent Droplets in Highly Scattering Turbid Media,'' Science **264**, 1913–1915 (1994).
[16]J. Watson, P. Georges, T. Lépine, B. Alonzi, and A. Brun, ''Imaging in diffuse media with ultrafast degenerate optical parametric amplification,'' Opt. Lett. **20**, 231–233 (1995).
[17]D. Contini, H. Liszka, A. Sassaroli, and G. Zaccanti, ''Imaging of highly turbid media by the absorption method,'' Appl. Opt. **35**, 2315–2324 (1996).
[18]P. N. Den Outer, Th. M. Nieuwenhuizen, and A. Lagendijk, ''Location of objects in multiple-scattering media,'' J. Opt. Soc. Am. A **10**, 1209–1218 (1993).
[19]A. Ishimaru, *Wave Propagation and Scattering in Random Media* (Academic, New York, 1978).
[20]H. C. van de Hulst, *Multiple Light Scattering* (Academic, New York, 1980).
[21]A. Yodh and B. Chance, ''Spectroscopy and Imaging with Diffusing Light,'' Phys. Today **48**, 34–40 (1995).
[22]M. Suzuki, ''General theory of fractal path integrals with applications to many-body theories and statistical physics,'' J. Math. Phys. **32**, 400–407 (1991).
[23]H. De Raedt and K. Michielsen, ''Algorithm to solve the time-dependent Schrödinger equation for a charged particle in an inhomogeneous magnetic field: Application to the Aharonov-Bohm effect,'' Comput. Phys. **8**, 600–607 (1994).
[24]G. D. Smith, *Numerical solution of partial differential equations* (Clarendon, Oxford, 1985).
[25]H. De Raedt and B. De Raedt, ''Applications of the Generalized Trotter Formula,'' Phys. Rev. A **28**, 3575–3580 (1983).
[26]M. Suzuki, ''Decomposition formulas of exponential operators and Lie exponentials with some applications to quantum mechanics and statistical physics,'' J. Math. Phys. **26**, 601–612 (1985).
[27]W. A. Press, B. P. Flannery, S. A. Teukolsky, and W. T. Vetterling, *Numerical Recipes* (Cambridge U.P., Cambridge, 1986).
[28]H. De Raedt, ''Product Formula Algorithms for Solving the Time-Dependent Schrödinger Equation,'' Comput. Phys. Rep. **7**, 1–72 (1987).
[29]M. Abramowitz and I. A. Stegun (eds.), *Handbook of Mathematical Functions* (National Bureau of Standards, Washington DC, 1964).
[30]B. C. Wilson and G. Adam, ''A Monte Carlo model for the absorption and flux distribution of light in tissue,'' Med. Phys. **10**, 824–830 (1983).
[31]P. van der Zee and D. T. Delpy, ''Simulation of the point spread function for light in tissue by a Monte Carlo technique,'' Adv. Exp. Med. Biol. **215**, 179–191 (1987).
[32]Y. Hasegawa, Y. Yamada, M. Tamura, and Y. Nomura, ''Monte Carlo simulation of light transmission through living tissues,'' Appl. Opt. **30**, 4515–4520 (1991).
[33]J. C. Hebden and R. A. Kruger, ''Transillumination imaging performance: A time of flight imaging system,'' Med. Phys. **17**, 351–356 (1990).
[34]E. B. de Haller and C. Depeursinge, ''Simulation of time-resolved breast transillumination,'' Med. Biol. Eng. Comp. **31**, 165–170 (1993).
[35]R. Graaff, M. H. Koelink, F. F. M. de Mul, W. G. Zijlstra, A. C. M. Dassel, and J. G. Aarnoudse, ''Condensed Monte Carlo simulations for the description of light transport,'' Appl. Opt. **32**, 426–434 (1993).
[36]R. F. Bonner, R. Nossal, R. Havlin, and G. H. Weiss, ''Model for photon migration in turbid biological media,'' J. Opt. Soc. Am. A **4**, 423–432 (1987).
[37]A. H. Gandjbakhcke, H. Taitelbaum, and G. H. Weiss, ''Random walk analysis of time-resolved transillumination measurements in optical imaging,'' Physica A **200**, 212–221 (1993).
[38]M. S. Patterson, B. Chance, and B. C. Wilson, ''Time resolved reflectance and transmittance for the noninvasive measurement of tissue optical properties,'' Appl. Opt. **28**, 2331–2336 (1989).
[39]S. R. Arridge, M. Schweiger, M. Hiraoka, and D. T. Delpy, ''A finite element approach for modeling photon transport in tissue,'' Med. Phys. **20**, 299–309 (1993).
[40]M. Schweiger, S. R. Arridge, M. Hiraoka, and D. T. Delpy, ''The finite element method for the propagation of light in scattering media: Boundary and source conditions,'' Med. Phys. **22**, 1779–1792 (1995).
[41]S. R. Arridge and M. Schweiger, ''Direct calculation of the moments of the distribution of photon time of flight in tissue with a finite element method,'' Appl. Opt. **34**, 2683–2687 (1995).
[42]R. Berg, S. Andersson-Engels, O. Jarlman, and S. Svanberg, ''Time-gated viewing studies on tissuelike phantoms,'' Appl. Opt. **35**, 3432–3440 (1996).
[43]H. De Raedt and K. Michielsen, preprint submitted to J. Math. Phys.
[44]K. Symanzik, ''Proof and Refinements of an Inequality of Feynman,'' J. Math. Phys. **6**, 1155–1156 (1965).
[45]V. G. Peters, D. R. Wyman, M. S. Patterson, and G. L. Frank, ''Optical properties of normal and diseased human breast tissues in the visible and near infrared,'' Phys. Med. Biol. **9**, 1317–1334 (1990).
[46]H. Key, E. R. Davies, P. C. Jackson, and P. N. T. Wells, ''Optical attenuation characteristics of breast tissues at visible and near-infrared wavelengths,'' Phys. Med. Biol. **36**, 579–590 (1991).
[47]K. Suzuki, Y. Yamashita, K. Ohta, and B. Chance, ''Quantitative measurement of optical parameters in the breast using time-resolved spectroscopy,'' Invest. Radiol. **29**, 410–414 (1994).